

## Estimating regional fluxes of CO<sub>2</sub> and CH<sub>4</sub> using space-borne observations of XCH<sub>4</sub> : XCO<sub>2</sub>

A. Fraser<sup>1</sup>, P. I. Palmer<sup>1</sup>, L. Feng<sup>1</sup>, H. Bösch<sup>2</sup>, R. Parker<sup>2</sup>, E. J. Dlugokencky<sup>3</sup>,  
P. B. Krummel<sup>4</sup>, and R. L. Langenfelds<sup>4</sup>

<sup>1</sup>School of GeoSciences, University of Edinburgh, UK

<sup>2</sup>Department of Physics and Astronomy, University of Leicester, Leicester, UK

<sup>3</sup>US National Oceanic and Atmospheric Administration, Global Monitoring Division, Earth System Research Laboratory, Boulder, Colorado, USA

<sup>4</sup>Centre for Australian Weather and Climate Research, CSIRO Marine and Atmospheric Research, Aspendale, Victoria, Australia

*Correspondence to:* P. I. Palmer (paul.palmer@ed.ac.uk)

**Abstract.** We use the GEOS-Chem global 3-D atmospheric chemistry transport model to interpret XCH<sub>4</sub> : XCO<sub>2</sub> column ratios retrieved from the Japanese Greenhouse gases Observing SATellite (GOSAT). The advantage of these data over CO<sub>2</sub> and CH<sub>4</sub> columns retrieved independently using a full physics optimal estimation algorithm is that they suffer less from scattering-related regional biases. We show the model is able to reproduce observed global and regional spatial (mean bias = 0.7 %) and temporal variations (global  $r^2 = 0.92$ ) of this ratio with a model bias  $< 2.5$  %. We also show these variations are driven by emissions of CO<sub>2</sub> and CH<sub>4</sub> that are typically six months out of phase which may reduce the sensitivity of the ratio to changes in either gas. To simultaneously estimate fluxes of CO<sub>2</sub> and CH<sub>4</sub> we use a maximum likelihood estimation approach. We use two approaches to resolve independent flux estimates of these two gases using GOSAT observations of XCH<sub>4</sub> : XCO<sub>2</sub>: (1) the a priori error covariance between CO<sub>2</sub> and CH<sub>4</sub> describing common source from biomass burning; and (2) also fitting independent surface atmospheric measurements of CH<sub>4</sub> and CO<sub>2</sub> mole fraction that provide additional constraints, improving the effectiveness of the observed GOSAT ratio to constrain fluxes. We demonstrate the impact of these two approaches using numerical experiments. A posteriori flux estimates inferred using only the GOSAT ratios and taking advantage of the error covariance due to biomass burning are not consistent with the true fluxes in our experiments, as the inversion system cannot judge which species' fluxes to adjust. This reflects the weak dependence of XCH<sub>4</sub> : XCO<sub>2</sub> on biomass burning. We find that adding the surface data effectively provides an “anchor” to the inversion that dramatically improves the ability of the GOSAT ratios to infer both CH<sub>4</sub> and CO<sub>2</sub> fluxes. We show that the regional flux estimates inferred from GOSAT XCH<sub>4</sub> : XCO<sub>2</sub> ratios together with the surface mole fraction data during 2010 are

typically consistent or better than the corresponding values inferred from fitting  $XCH_4$  or the full-physics  $XCO_2$  data products, as judged by a posteriori uncertainties. We show the fluxes inferred from the ratio measurements perform best over regions where there is a large seasonal cycle such as Tropical South America for which we report a small but significant annual source of  $CO_2$  compared to a small annual sink inferred from the  $XCO_2$  data. We argue that given that the ratio measurements are less compromised by systematic error than the full physics data products the resulting a posteriori estimates and uncertainties provide a more faithful description of the truth. Based on our analysis we also argue that by using the ratios we may be reaching the current limits on the precision of observed space-based data.

## 1 Introduction

Space-borne atmospheric column measurements of  $CO_2$  and  $CH_4$  have the potential to improve our quantitative understanding of their surface fluxes and to underpin the development of testable climate policies. For these data to address these potential applications the column measurements have to meet strict precision requirements, reflecting small signals from surface fluxes (a few percent of the column amount) compared to the variations due to atmospheric transport. Any uncharacterized systematic error in these measurements compromises the ability of these data to infer surface fluxes. The  $CO_2$  inverse problem is particularly sensitive to these systematic errors acting on length scales of  $10^3$ – $10^4$  km, in between the spatial scales of numerical models and those observed by the sparse network of well characterized upward-looking Fourier transform spectrometers, regional aircraft, and the network of ground-based measurements. Here, we develop a method to infer simultaneous regional  $CO_2$  and  $CH_4$  flux estimates (Fig. 1) from the ratio of  $CH_4$  and  $CO_2$  dry-air mole fraction measurements ( $XCH_4 : XCO_2$ ) retrieved from the Japanese Greenhouse gases Observing SATellite (GOSAT) using the proxy approach (based on University of Leicester proxy  $XCH_4$  v4), which is less prone to systematic error from aerosols than the full physics approach (Schepers et al., 2012).

Two methods have been used to retrieve  $CO_2$  and  $CH_4$  columns from calibrated GOSAT L1B spectra: the “full physics” and the “proxy” methods (Cogan et al., 2012; Parker et al., 2011). The full physics method uses an optimal estimation approach and incorporates a rigorous treatment of the atmospheric radiative transfer including the effects of clouds and aerosols. This method uses optimized spectral windows to fit  $CO_2$  and  $CH_4$ . The main advantage of this approach is the error characterization of the a posteriori state vector, and the main disadvantage is having to accurately characterize the atmospheric aerosol for the radiative transfer calculation. The proxy method, used to infer  $CH_4$  columns, fits both gases in nearby spectral windows with the assumption that any fitting artefacts common to both gases (e.g. aerosol and clouds) will be removed by taking the ratio of the two gases. This method is simpler than the full physics approach and more robust against scattering, and as a result many more retrievals are possible from the GOSAT spectra. Interpretation of this

ratio has in the past relied on scaling it with a model  $\text{CO}_2$  column so that any erroneous model information about  $\text{CO}_2$  can influence the interpretation of the GOSAT  $\text{CH}_4$  columns (e.g. Parker et al., 2011; Fraser et al., 2013). We propose a method to simultaneously optimize  $\text{CH}_4$  and  $\text{CO}_2$  fluxes using the retrieved  $\text{XCH}_4 : \text{XCO}_2$  ratio. This eliminates the need for a  $\text{CO}_2$  model, removing the impact of model uncertainty on the retrieved methane columns, and increases the number of observations available to constrain  $\text{CO}_2$  fluxes (Fig. 2).

In the following section we describe the space-borne and ground-based data used in our experiments. In Sect. 3 we describe the GEOS-Chem chemical transport model, and the maximum likelihood estimation (MLE) approach developed for this work. In Sect. 4 we report the GOSAT and model spatial and temporal distributions of  $\text{XCH}_4 : \text{XCO}_2$  ratios (Sect. 4.1), we test the MLE approach using a series of Observing System Simulation Experiments (OSSEs, Sect. 4.2) and present inversion results (Sect. 4.3). We conclude the paper in Sect. 5.

## 2 Data

### 2.1 GOSAT $\text{CO}_2$ and $\text{CH}_4$ atmospheric column-averaged mole fraction measurements

GOSAT was launched in 2009 by the Japanese Space Agency in a sun-synchronous orbit with an equatorial local overpass time of 13:00 LT, providing global coverage every three days (Kuze et al., 2009). GOSAT includes two instruments: TANSO-FTS (Thermal and Near Infrared Sensor for carbon Observations – Fourier Transform Spectrometer) and TANSO-CAI (TANSO – Cloud and Aerosol Imager). The TANSO-FTS instrument provides short-wave infrared (SWIR) radiances from which dry-air mole fraction observations of  $\text{CO}_2$  and  $\text{CH}_4$ ,  $\text{XCO}_2$  and  $\text{XCH}_4$ , can be retrieved.

We provide a brief description of the proxy retrieval algorithm used for  $\text{XCO}_2$  and  $\text{XCH}_4$  and refer the reader to a detailed description (Parker et al., 2011). Here, we only consider nadir measurements.  $\text{XCH}_4$  and  $\text{XCO}_2$  are retrieved at 1.65  $\mu\text{m}$  and 1.61  $\mu\text{m}$ , respectively. Past work has used this approach to infer observations of  $\text{XCH}_4$  by scaling it by  $\text{XCO}_2$ , using  $\text{XCO}_2$  as a proxy for the light path through the atmosphere. The mole fraction of  $\text{XCH}_4$  is then obtained using a model estimate for  $\text{XCO}_2$  so that  $\text{XCH}_4^{\text{PROXY}} = \left[ \frac{\text{XCH}_4}{\text{XCO}_2} \right]^{\text{GOSAT}} \times \text{XCO}_2^{\text{MODEL}}$ . However, using an inaccurate model of atmospheric  $\text{CO}_2$  will introduce erroneous variability and bias in resulting values for  $\text{XCH}_4^{\text{PROXY}}$ . In this work we use the ratio  $\left[ \frac{\text{XCH}_4}{\text{XCO}_2} \right]^{\text{GOSAT}}$  directly, removing the requirement of model  $\text{XCO}_2$ .

We use cloud-screening and  $\chi^2$  quality-of-fit criteria, recommended by Parker et al. (2011), to filter retrieved  $\text{XCH}_4 : \text{XCO}_2$  ratios. GOSAT surface pressure values, retrieved from the  $\text{O}_2$  A-band for scenes with an estimated  $\text{SNR} > 50$ , are compared with colocated ECMWF surface pressure data. We discard cloudy scenes where the difference is  $> 30$  hPa. We also discard data: 1) with solar zenith angles  $> 70^\circ$  to remove data affected by long atmospheric path lengths and large incidence angles; 2) poleward of  $60^\circ$  latitude to minimize the model error due to the stratosphere; and 3) taken at medium-gain (Fraser et al., 2013) as it can potentially include different biases than the high-gain

data, and there are currently no sites to validate these medium gain data. Here, we use version 4 of the proxy  $XCH_4$  data, while our previous analysis (Fraser et al., 2013) used version 3 of the data. Version 4 of the data includes an update to the GOSAT L1B data and its radiometric degradation, an update to the spectroscopic inputs and improvements to the a priori. Details about the validation of this data product can be found in the ESA GHG-CCI Product Validation and Intercomparison Report (ESA GHG-CCI PVIR) under section 6.2.3. The fractional differences between the final data products of v3 and v4, especially for  $XCH_4 : XCO_2$ , are small. For the full physics retrievals, due to the necessity of removing many more scenes affected by aerosol, the post-filtering requirements are much more stringent. This includes filters based on the retrieved aerosol amounts, geophysical characteristics of the scene (such as albedo and topography) and the consistency between Band 2 and Band 3  $XCO_2$ . Figure 2 shows that the proxy method typically provides twice the number of observations available from the full physics approach.

## 2.2 In situ surface atmosphere mole fraction measurements

As described in Sect. 4.2, we use these in situ data as independent constraints for  $CH_4$  and  $CO_2$  emission estimates, improving the ability of the GOSAT proxy ratio to act as a constraint on both  $CH_4$  and  $CO_2$  flux estimates. We assimilate data from 45 sites of the NOAA Earth System Research Laboratory (ESRL), Global Monitoring Division, version 28 August 2013 (Dlugokencky et al., 2013); nine sites from the CSIRO Global Atmospheric Sampling Laboratory (GASLAB), released August 2013 (Francey et al., 1996); and two sites from Environment Canada’s Greenhouse Gas Measurement Program (EC), released August 2013 (Worthy et al., 2003). Weekly air samples from all three networks are collected from sites distributed globally and data are reported on the NOAA 2004 ( $CH_4$ , all networks) and WMO X2007 ( $CO_2$ , ESRL, CSIRO) or WMO X83 ( $CO_2$ , EC) mole fraction scales. Figure 1 shows the location of the sites used in this work. Three sites are in both the ESRL and GASLAB networks: Mauna Loa, Hawaii; Cape Grim, Tasmania; and the South Pole. Alert, Nunavut is in all three networks. At these sites we average the data from the available networks, leaving 51 individual sites.

## 3 Models

### 3.1 The GEOS-Chem transport model

We use version v9-01-03 of the GEOS-Chem global 3-D atmospheric chemistry transport model (Bey et al., 2001), driven by assimilated meteorological fields from the NASA Global Modeling and Assimilation Office (version 5), to interpret observed variations of GOSAT proxy ratio measurements. We use the GEOS-5 meteorology at a horizontal resolution of  $4^\circ$  (latitude)  $\times$   $5^\circ$  (longitude) with 47 vertical levels that span from the surface to the mesosphere, with typically 35 levels in the troposphere.

The CH<sub>4</sub> and CO<sub>2</sub> simulations are described and evaluated against correlative data in Fraser et al. (2011) and Feng et al. (2011), respectively. Table 1 and Fig. 3 show the a priori global annual flux estimates and temporal distribution of CH<sub>4</sub> and CO<sub>2</sub> fluxes, respectively. The main atmospheric sink of CH<sub>4</sub> is the hydroxyl radical and is described in the troposphere by monthly mean 3-D fields generated by a full chemistry version of the model, which correspond to a methyl chloroform lifetime of 6.3 years. Loss rates for methane in the stratosphere are adapted from a 2-D stratospheric model (Wang et al., 2004).

### 3.2 The MAP inverse model

We use an inverse model that finds the maximum a posteriori (MAP) solution (Rodgers, 2000) to simultaneously optimize the magnitude of the CH<sub>4</sub> and CO<sub>2</sub> flux estimates by fitting the a priori emission estimates, via the GEOS-Chem model (described above) to observations of GOSAT XCH<sub>4</sub> : XCO<sub>2</sub> ratios and in situ CH<sub>4</sub> and/or CO<sub>2</sub> mole fraction measurements. The MAP solution  $\hat{\mathbf{x}}$  and the associated error covariance  $\hat{\mathbf{S}}$  can be written as:

$$\hat{\mathbf{x}} = \mathbf{x}_a + (\mathbf{K}^T \mathbf{S}_\epsilon^{-1} \mathbf{K} + \mathbf{S}_a^{-1})^{-1} \mathbf{K}^T \mathbf{S}_\epsilon^{-1} (\mathbf{y} - \mathbf{K} \mathbf{x}_a) \quad (1)$$

$$\hat{\mathbf{S}} = (\mathbf{K}^T \mathbf{S}_\epsilon^{-1} \mathbf{K} + \mathbf{S}_a^{-1})^{-1}, \quad (2)$$

where  $\mathbf{x}_a$  denotes the a priori vector, including a priori flux estimates of CO<sub>2</sub> and CH<sub>4</sub>;  $\mathbf{y}$  denotes the measurement vector, including the GOSAT XCH<sub>4</sub> : XCO<sub>2</sub> ratios and in situ CH<sub>4</sub> and/or CO<sub>2</sub> observations;  $\mathbf{K}$  denotes the Jacobian matrix, describing the sensitivity of model atmospheric concentrations to changes in the surface fluxes;  $\mathbf{S}_a$  denotes the a priori flux error covariance matrix; and  $\mathbf{S}_\epsilon$  denotes the observation error covariance matrix. The superscripts T and  $-1$  denote the matrix transpose and inverse operations, respectively.

For our implementation,  $\mathbf{x}_a$  includes monthly CH<sub>4</sub> and CO<sub>2</sub> in 13 geographical regions (Fig. 1). We separate the fluxes into contributions from biomass burning, the biosphere, and anthropogenic activities. For CH<sub>4</sub>, the biosphere includes contributions from wetlands, oceans, termites, hydrates, and the soil sink; and the anthropogenic activities include ruminant animals, coal mining, oil and natural gas production, landfills, and rice. For CO<sub>2</sub>, the biosphere includes the land and ocean fluxes, and the anthropogenic activities include fossil fuel combustion. We optimize for the total flux from the global ice and ocean regions. The state vector has 840 elements made up of 11 continental regions including three sectors each for CO<sub>2</sub> and CH<sub>4</sub> for 12 months, and for ice and ocean regions for the two gases for the 12 months.

We construct  $\mathbf{S}_a$  as a diagonal matrix with the elements being the square of the error in the a priori fluxes, which we assume, guided by empirical studies, to be 100 % for the biospheric fluxes and 50 % for the biomass burning and anthropogenic fluxes. We assume no temporal correlation between fluxes in the same region or sector. We generally assume no correlation between CH<sub>4</sub> and CO<sub>2</sub> flux errors because they are not co-emitted, with the exception of biomass burning for which we include

a region-specific correlation with a mean value of 0.8 following previous empirical work (Palmer et al., 2006). As we discuss below this correlation is a weak constraint for separating  $\text{CH}_4$  and  $\text{CO}_2$  from the observed  $\text{XCH}_4 : \text{XCO}_2$  column ratio.

The measurement vector  $\mathbf{y}$  includes a spatial and temporal average of GOSAT  $\text{XCH}_4 : \text{XCO}_2$  ratio measurements. We average the data into monthly means for the  $4^\circ \times 5^\circ$  grid boxes of GEOS-Chem, which ensures a reasonable number of measurements for each month and increases the signal to noise of the observed ratio, as described below; we include the associated error in  $\mathbf{S}_\epsilon$ . Estimates inferred using finer temporal and spatial bins tend to be noisier, largely reflecting changes in the measurement coverage from clouds and aerosols, but still produce consistent results shown here when they are averaged monthly and on the model grid. For some experiments,  $\mathbf{y}$  also includes in situ surface measurements of  $\text{CH}_4$  and/or  $\text{CO}_2$ .

We construct  $\mathbf{S}_\epsilon$  as a diagonal matrix with the diagonal elements being the standard error of the mean measurement error. For GOSAT, we use the a posteriori retrieval error from the v4 data product as described above. For surface data the measurement error is the standard error of the monthly mean calculated from the observations made over that month (Fraser et al., 2013). We also include a model transport error for each individual measurement error. For both the GOSAT ratio measurements and surface in situ data we describe this error as 0.25 % for  $(\text{X})\text{CO}_2$  (Feng et al., 2011) and 0.5 % for  $(\text{X})\text{CH}_4$  (Wang et al., 2004). When we average we sum these errors in quadrature.

The Jacobian matrix,  $\mathbf{K}$ , is constructed from forward runs of the model where the fluxes in each region and for each sector are perturbed by 1 Gt for  $\text{CO}_2$  or 1 Tg for  $\text{CH}_4$ . The model is then sampled at the time and location of the observations, smoothed using GOSAT averaging kernels, and these sensitivities are averaged into monthly and regional means.

## 4 Results

### 4.1 Forward modelling of GOSAT $\text{XCH}_4 : \text{XCO}_2$ ratios

Figure 3 shows that for many geographical regions  $\text{CH}_4$  and  $\text{CO}_2$  flux estimates are six months out of phase, reflecting seasonal changes in wetland emissions of  $\text{CH}_4$  and terrestrial  $\text{CO}_2$  fluxes. The opposing seasonal cycles will result in a partial cancellation of individual gas variations, and consequently may reduce the sensitivity of the ratio to variations in either gas.

Figure 4 shows the observed spatial variability of the annual mean  $\text{XCH}_4 : \text{XCO}_2$  ratio is due mainly to  $\text{XCH}_4$  variations. Common features to both the model and data include the interhemispheric gradient in the ratio and localized features due to orography, e.g., the Himalayan mountain range. The GEOS-Chem model reproduces the spatial pattern of the GOSAT ratio observations within  $\simeq 2.5\%$ . The model has a negative bias over the tropics (1–2%), which is largely due to the model positive bias for  $\text{XCO}_2$  that reflects errors in the a priori natural flux inventories. This figure illustrates the demanding accuracy and precision requirements associated with this space-borne

measurement if it is to become a useful constraint for carbon cycle science. The monthly variation  
190 of observed values, here shown as the  $1-\sigma$  value expressed as a percentage about the annual mean, is  
smaller for the  $XCH_4 : XCO_2$  ratios for which scattering and other biases are removed than  $XCH_4$   
or  $XCO_2$ .

Figure 5 shows that the model can typically capture 70 % of the observed temporal variability of  
 $XCH_4 : XCO_2$  over different geographical regions. Over most regions we find the model has a small  
195 but growing negative bias, reflecting its overestimation of the  $CO_2$  growth rate. The model generally  
agrees best with GOSAT in the Northern Hemisphere extra-tropics, and the worst over Tropical  
South America, where we know the model underestimates the  $CO_2$  biological uptake. While  $XCH_4$   
variations determine the spatial distribution of the GOSAT  $XCH_4 : XCO_2$  ratio, we find that  $XCO_2$   
determines its seasonal cycle. This is particularly noticeable over boreal regions and Europe, where  
200 the peak in the ratio in the second half of the year is a result of decreasing  $XCO_2$  due to increased  
uptake from the biosphere.

Figure 5 also illustrates the importance of using the ratio instead of the contributory columns. Both  
 $XCH_4$  and  $XCO_2$  are too noisy (due to variations in the atmosphere and surface) by themselves but  
common retrieval errors will cancel out in the ratio. Please note that the  $XCH_4$  and  $XCO_2$  plotted  
205 here are not the final data products from GOSAT, but the intermediary products from which the ratio  
is calculated. Comparing this figure to Fig. 5 in Cogan et al. (2012) and Fig. 3 in Parker et al. (2011)  
shows that the regional bias between GOSAT and the model is much smaller in the ratio than in the  
individual species. While GEOS-Chem tends to underestimate the GOSAT ratio, the bias is more or  
less consistent between regions, which is not the case for either  $XCO_2$  or  $XCH_4$ .

## 210 4.2 Inverse modelling of GOSAT $XCH_4 : XCO_2$ ratios: OSSEs

We use OSSEs, realistic numerical experiments, to characterize the method we use to estimate si-  
multaneously  $CO_2$  and  $CH_4$  regional fluxes from GOSAT  $XCH_4 : XCO_2$  ratios. For all these exper-  
iments, we sample the model at the location of the clear-sky GOSAT observations, apply GOSAT  
averaging kernels, and add, as a minimum, random error based on actual GOSAT measurements.  
215 Similarly, we sample the model at the time and location of the surface observations and add charac-  
teristic random noise informed by the data.

We conduct four broad sets of OSSEs: (1) those that use only the GOSAT  $XCH_4 : XCO_2$  ratios,  
(2) those that use the GOSAT data and in situ measurements of  $CH_4$  and/or  $CO_2$ , (3) those that use  
the best setup from (2) and vary the a priori fluxes, and (4) as (3) but including regional bias.

220 Figure 6a and b show the results from experimental set (1). First, we assume that the a priori  
fluxes equal the true fluxes, allowing us to assess the level of numerical noise in the closed-loop  
system. We find that after setting the a priori to the true fluxes there is only a small mean difference  
between a posteriori and true fluxes that is within the uncertainty of the a posteriori fluxes. We then  
assume that the a priori fluxes are scaled by 20 % relative to the truth, allowing us to assess the

225 efficacy with which the synthetic observations can recover the true flux estimates. Because  $\text{CO}_2$  and  $\text{CH}_4$  fluxes have different geographical distributions the simultaneous increase will not necessarily cancel out in the ratio. For this scaling experiment the observing system reconciles the model minus observation difference by simultaneously changing the  $\text{CH}_4$  and  $\text{CO}_2$  fluxes that are not always within the a posteriori flux uncertainties, which we attribute to the fact that there is no additional  
 230 information about allocating this difference to a particular gas.

Figure 6c–e shows results from experimental set (2). Adding either  $\text{CH}_4$  or  $\text{CO}_2$  surface observations to the measurement vector reduces the bias between the a posteriori and true fluxes (by up to nearly 100%), but also reduces the error reduction of the other species. We find that assimilating both  $\text{CH}_4$  and  $\text{CO}_2$  surface observations gives the smallest difference from the truth and the largest  
 235 error reductions; we adopt this as our control experimental setup in the following sections. We accept the larger standard deviations as the fluxes are closer to the truth. For reference, using only the surface data returns error reductions of approximately 23 % for both species (not shown). Figure 7 shows the results from experimental set (3). This control observing system can return the true fluxes for a wide array of varying  $\text{CH}_4$  and  $\text{CO}_2$  fluxes for most geographical regions.

240 In experiment set (4) (not shown) we assess the impact of a prescribed observation bias to the GOSAT data on the a posteriori flux estimates; assuming that the surface data is unbiased or at least can be identified readily via ongoing calibration/validation activities. We assume a latitudinally-varying bias that is superimposed onto the “true” atmospheric measurements plus random error ( $0.005 \text{ ppbppm}^{-1}$ ) for the monthly gridded measurement vector. To describe the latitudinal bias,  
 245 we use a second-order polynomial with a minimum at the South Pole and a maximum at the North Pole; our choice of this polynomial is based on the bias between the model and GOSAT data. This bias ranges from  $-0.08$  to  $0.06 \pm 0.005 \text{ ppbppm}^{-1}$ . We conduct two parallel experiments: i) we assume the data was unbiased and ii) we assume and fit a fourth-degree polynomial as a function of latitude to the mean annual difference between the model and data. We find that using higher degree  
 250 polynomials did not significantly change our results. For experiment 4i), the resulting  $\text{CH}_4$  and  $\text{CO}_2$  fluxes are up to 10 Tg and 0.4 Gt different from the true fluxes, respectively. For experiment 4ii), we find the bias correction returns values that are closer to the true fluxes.

### 4.3 Analysis of GOSAT $\text{XCH}_4 : \text{XCO}_2$ ratios

Figure 8 and Table 2 show flux estimates inferred from GOSAT  $\text{XCH}_4 : \text{XCO}_2$  data and surface mole  
 255 fraction observations of  $\text{CH}_4$  and  $\text{CO}_2$  (Sect. 2), and independent flux estimates of  $\text{CH}_4$  and  $\text{CO}_2$  inferred using an ensemble Kalman filter (EnKF) from GOSAT  $\text{XCH}_4$  proxy data (Fraser et al., 2013) and  $\text{XCO}_2$  full physics data together with the corresponding surface stations (Feng et al., 2011; Chevallier et al., 2014).

For  $\text{CH}_4$ , the general tendency of a posteriori fluxes, relative to a priori values, are consistent  
 260 between the  $\text{XCH}_4 : \text{XCO}_2$  ratio and the proxy  $\text{XCH}_4$  data, but based on a posteriori uncertainties



the magnitude of these fluxes can be statistically different. The ratio infers larger emissions from Tropical South America, Northern Africa, and Temperate Eurasia. Error reductions resulting from assimilating  $XCH_4 : XCO_2$  ratio data are typically 30 % but can be up to 60 % (Temperate Eurasia). For some regions, the error reduction from using the ratio is larger than from using the individual gas but for others the reduction is smaller. Geographical regions with notable improvements in our understanding from assimilating the ratio data include Tropical and Temperate South America, Northern Africa, and Temperate Eurasia. These regions all have observed seasonal cycles in the ratio that are larger than a few percent of the annual mean, allowing the ratio data to better inform the a priori. Strictly speaking we cannot compare directly the  $CH_4$  flux estimated reported by Fraser et al. (2013) and those inferred from the  $XCH_4 : XCO_2$  ratio data. As noted above we are using a newer version of the proxy retrieval that includes updated a priori information particularly for stratospheric  $CH_4$  concentrations and updates to the retrieval grid and spectroscopic input, resulting in 5–10 % more clear-sky measurements; we are using a newer version of the GEOS-Chem transport model; and most importantly we treat the measurements differently, reflecting the difficulty in the small observed changes in the  $XCH_4 : XCO_2$  ratio data.

For  $CO_2$ , a posteriori fluxes inferred from the GOSAT ratio can be statistically different to those inferred from the EnKF inversion, including Tropical South America, Southern Africa, Boreal Eurasia, Tropical Asia, and Australasia. These differences between the inversion largely reflect the larger volume of  $XCH_4 : XCO_2$  ratio data resulting in better spatial and temporal coverage (Fig. 2). We may also expect the largest differences for regions where we believe there are the greatest biases in the proxy  $XCH_4$  and full physics  $XCO_2$  retrievals. We find that the associated error reductions for the  $CO_2$  fluxes inferred from the  $XCH_4 : XCO_2$  ratio data are generally larger than those for  $CH_4$ , and are different from those inferred from the EnKF inversion.

## 5 Concluding remarks

We have interpreted measurements of  $XCH_4 : XCO_2$  from GOSAT in which  $XCH_4$  and  $XCO_2$  are retrieved in nearby spectral windows under the assumption that their ratio will largely remove common sources of biases. By interpreting the ratio directly we minimize any bias introduced by model  $XCO_2$ ; although we acknowledge other sources of model bias remain. A major advantage of the ratio is this data product does not suffer from the measurement bias that can befall the full physics  $XCO_2$  and  $CH_4$  data. Another advantage is that the volume of these data is greater than their full physics counterpart. While the ratio benefits from these three advantages, the difference between model and observed quantities are much smaller (typically  $< \pm 2\%$ ) than the corresponding changes in  $XCO_2$  or  $XCH_4$  and consequently comparable in magnitude to other sources of error, e.g. model transport error, that cannot easily be characterized and removed. By using the ratio we may be reaching the limitations on the precision of these data and our ability to interpret them

using current-day transport models. However, over particular geographical regions we find there are seasonally varying GOSAT minus model ratio differences that are large enough to be exploited, e.g., Tropical South America and Tropical Asia.

Using a series of numerical experiments we showed that the simultaneous estimation of CO<sub>2</sub> and CH<sub>4</sub> fluxes using the GOSAT ratio is possible with the information split as a function of the a priori uncertainties, however the inversion system returns unphysical fluxes in some regions. We showed that including surface mole fraction measurements of CO<sub>2</sub> and CH<sub>4</sub> in the measurement vector provides an “anchor” for the inversion, and that the combined GOSAT and surface data can distinguish between CO<sub>2</sub> and CH<sub>4</sub> flux adjustments.

Using real data for 2010 we showed that the combination of the GOSAT XCH<sub>4</sub> : XCO<sub>2</sub> ratio and the surface mole fraction data led to comparable flux estimates inferred from the proxy XCH<sub>4</sub> and full physics XCO<sub>2</sub> data, but outcompeted these individual data products over geographical regions where there was a seasonal cycle larger than a few percent of the annual mean. For instance, over Tropical South America we found a small but significant emission of CO<sub>2</sub> while analysis of the full physics XCO<sub>2</sub> showed a small sink term. Analysis of the ratio led to slightly larger reductions globally, and in some regions, primarily in the tropics, much larger reductions in uncertainty of CO<sub>2</sub> and CH<sub>4</sub>. Given that the ratio data are less compromised by systematic biases than the proxy XCH<sub>4</sub> and full physics XCO<sub>2</sub> data products, we more generally argue that the corresponding a posteriori flux estimates and their uncertainties provide a more faithful description of regional fluxes.

The main reasons for using the XCH<sub>4</sub> : XCO<sub>2</sub> ratio is that it minimizes scattering and potentially other biases and significantly increases geographical coverage. Although CO<sub>2</sub> and CH<sub>4</sub> do not share many common sources that result in significant atmospheric covariance we have shown that: (1) the combined information from these two gases can be disentangled using other data, and (2) flux estimates inferred from the XCH<sub>4</sub> : XCO<sub>2</sub> ratio are an improvement over what can be achieved using observations of either full-physics XCO<sub>2</sub> or XCH<sub>4</sub>. Consequently, the use of space-borne observations of the XCH<sub>4</sub> : XCO<sub>2</sub> ratio will be of particular interest for estimating CO<sub>2</sub> surface fluxes over regions that are characterized by frequent cloud cover and high aerosol loading such as the tropics where the quality and coverage of full-physics XCO<sub>2</sub> retrieval approaches will be limited even for missions with spatial footprints smaller than GOSAT. This ratio approach could also be used in combination with other atmospheric tracers that help improve the source attribution of CO<sub>2</sub>, e.g., carbon monoxide, where the ensuing correlation is driven by incomplete combustion (Palmer et al., 2006). Space-borne mission concept development related to the carbon cycle should not only focus on the primary compound but also on any secondary compound that will help interpret the observed variability of that primary gas.

*Acknowledgements.* We thank Doug Worthy for the Environment Canada data. NOAA ESRL is supported by NOAA’s Climate Program Office; and CSIRO research at Cape Grim is supported by the Australian Bureau

of Meteorology. AF and RP were supported by the Natural Environment Research Council National Centre for Earth Observation (NCEO). LF was partly funded by the “Data Assimilation Project-Interfacing EO data with atmospheric and land surface models” ESA contract 4000104980/1-LG. HB, RP and LF also acknowledge  
335 funding by the ESA Climate Change Initiative (GHG-CCI). PIP gratefully acknowledges his Royal Society Wolfson Research Merit Award.

## References

- Bey, I., Jacob, D. J., Yantosca, R. M., Logan, J. A., Field, B., Fiore, A. M., Li, Q., Liu, H., Mickley, L. J., and  
 340 Schultz, M.: Global modeling of tropospheric chemistry with assimilated meteorology: Model description  
 and evaluation, *J. Geophys. Res.*, 106, 23,073–23,096, 2001a.
- Bloom, A. A., Palmer, P. I., Fraser, A., and Reay, D. S.: Seasonal variability of tropical wetland CH<sub>4</sub> emissions:  
 the role of the methanogen-available carbon pool, *Biogeosciences*, 9, 2821–2830, 10.5194/bg-9-2821-2012,  
 2012.
- 345 Chevallier, F., Palmer, P. I., Feng, L., Boesch, H., O'Dell, C., W., and Bousquet, P.: Toward robust and consistent  
 regional CO<sub>2</sub> flux estimates from in situ and spaceborne measurements of atmospheric CO<sub>2</sub>, *Geophys. Res.*  
*Lett.*, 1, 10.1002/2013GL058772, 2014.
- Cogan, A. J., Boesch, H., Parker, R. J., Feng, L., Palmer, P. I., Blavier, J.-F. L., Deutscher, N. M., Macatan-  
 gay, R., Notholt, J., Roehl, C., Warneke, T., and Wunch, D.: Atmospheric carbon dioxide retrieved from the  
 350 Greenhouse gases Observing SATellite (GOSAT): comparison with ground-based TCCON observations and  
 GEOS-Chem model calculations, *J. Geophys. Res.*, 117, D21301, 10.1029/2012JD018087, 2012.
- Dlugokencky, E. J., Lang, P. M., Crotwell, A., Masarie, K. A., and Crotwell, M.: Atmospheric methane dry air  
 mole fractions from the NOAA ESRL carbon cycle cooperative global air sampling network, 1983–2012,  
 Version: 2013-08-28, available at: [ftp://aftp.cmdl.noaa.gov/data/trace\\_gases/ch4/flask/surface/](ftp://aftp.cmdl.noaa.gov/data/trace_gases/ch4/flask/surface/) (last access:  
 355 September 2013), 2013.
- Feng, L., Palmer, P. I., Yang, Y., Yantosca, R. M., Kawa, S. R., Paris, J.-D., Matsueda, H., and Machida, T.:  
 Evaluating a 3-D transport model of atmospheric CO<sub>2</sub> using ground-based, aircraft, and space-borne data,  
*Atmos. Chem. Phys.*, 11, 2789–2803, 10.5194/acp-11-2789-2011, 2011.
- Francey, R. J., Steele, L. P., Langenfelds, R. L., Lucarelli, M. P., Allison, C. E., Beardsmore, D. J., Coram, S. A.,  
 360 Derek, N., de Silva, F. R., Etheridge, D. M., Fraser, P. J., Henry, R. J., Turner, B., Welch, E. D., Spencer, D. A.,  
 and Cooper, L. N.: Global Atmospheric Sampling Laboratory (GASLAB): supporting and extending the  
 Cape Grim trace gas programs, in: *Baseline Atmospheric Program (Australia)*, Bureau of Meteorology and  
 CSIRO Division of Atmospheric Research, Melbourne, Australia, 8–29, 1996.
- Fraser, A., Chan Miller, C., Palmer, P. I., Deutscher, N. M., Jones, N. B., and Griffith, D. W. T.: The Australian  
 365 methane budget: interpreting surface and train-borne measurements using a chemistry transport model, *J*  
*Geophys. Res.*, 116, D20306, 10.1029/2011JD015964, 2011.
- Fraser, A., Palmer, P. I., Feng, L., Boesch, H., Cogan, A., Parker, R., Dlugokencky, E. J., Fraser, P. J., Krum-  
 mel, P. B., Langenfelds, R. L., O'Doherty, S., Prinn, R. G., Steele, L. P., van der Schoot, M., and Weiss, R. F.:  
 Estimating regional methane surface fluxes: the relative importance of surface and GOSAT mole fraction  
 370 measurements, *Atmos. Chem. Phys.*, 13, 5697–5713, 10.5194/acp-13-5697-2013, 2013.
- Fung, I., John, J., Lerner, J., Matthews, E., Prather, M., Steele, L. P., and Fraser, P. J.: Three-dimensional model  
 synthesis of the global methane cycle, *J. Geophys. Res.*, 96, 13033–13065, 10.1029/91JD01247, 1991.
- Gurney, K. R., Law, R. M., Denning, A. S., Rayner, P. J., Baker, D., Bousquet, P., Bruhwiler, L., Chen, Y.-  
 H., Ciais, P., Fan, S., Fung, I. Y., Gloor, M., Heimann, M., Higuchi, K., John, J., Maki, T., Maksyutov, S.,  
 375 Masarie, K., Peylin, P., Prather, M., Pak, B. C., Randerson, J., Sarmiento, J., Taguchi, S., Takahashi, T.,  
 and Yuen, C.-W.: Towards robust regional estimates of CO<sub>2</sub> sources and sinks using atmospheric transport  
 models, *Nature*, 415, 626–630, 10.1038/415626a, 2002.

Houweling, S., Kaminski, T., Dentener, F., Lelieveld, J., and Heimann, M.: Inverse modeling of methane sources and sinks using the adjoint of a global transport model, *J. Geophys. Res.*, 104, 26137–26160, 10.1029/1999JD900428, 1999.

Kuze, A., Suto, H., Nakajima, M., and Hamazaki, T.: Thermal and near infrared sensor for carbon observation Fourier-transform spectrometer on the Greenhouse Gases Observing Satellite for greenhouse gases monitoring, *Appl. Optics*, 48, 6716–6733, 10.1364/AO.48.006716, 2009.

Oda, T. and Maksyutov, S.: A very high-resolution ( $1\text{km} \times 1\text{km}$ ) global fossil fuel  $\text{CO}_2$  emission inventory derived using a point source database and satellite observations of nighttime lights, *Atmos. Chem. Phys.*, 11, 543–556, 10.5194/acp-11-543-2011, 2011.

Olivier, J. G. J., van Aardenne, J. A., Dentener, F., Ganzeveld, L., and Peters, J. A. H. W.: Recent trends in global greenhouse gas emissions: regional trends and spatial distribution of key sources, in: *Non- $\text{CO}_2$  Greenhouse Gases (NCGG-4)*, edited by: van Amstel, A., Millpress, Rotterdam, 325–330, 2005.

Palmer, P., Suntharalingam, P., Jones, D., Jacob, D., Streets, D., Fu, Q., Vay, S., and Sachse, G.: Using  $\text{CO}_2$  : CO correlations to improve inverse analyses of carbon fluxes, *J. Geophys. Res.*, 111, D12318, 10.1029/2005JD006697, 2006.

Parker, R., Boesch, H., Cogan, A., Fraser, A., Feng, L., Palmer, P. I., Messerschmidt, J., Deutscher, N., Griffith, D. W., Notholt, J., Wennberg, P. O., and Wunch, D.: Methane observations from the Greenhouse Gases Observing SATellite: comparison to ground-based TCCON data and model calculations, *Geophys. Res. Lett.*, 38, L15807, 10.1029/2011GL047871, 2011.

Randerson, J., Thompson, M., Conway, T., Fung, I., and Field, C.: The contribution of terrestrial sources and sinks to trends in the seasonal cycle of atmospheric carbon dioxide, *Global Biogeochem. Cy.*, 11, 535–560, 1997.

Rodgers, C. D.: *Inverse Methods for Atmospheric Sounding: Theory and Practice*, World Scientific Publishing, River Edge, NJ, 2000.

Schepers, D., Guerlet, S., Butz, A., Landgraf, J., Frankenberg, C., Hasekamp, O., Blavier, J.-F., Deutscher, N. M., Griffith, D. W. T., Hase, F., Kyro, E., Morino, I., Sherlock, V., Sussmann, R., and Aben, I.: Methane retrievals from Greenhouse Gases Observing Satellite (GOSAT) shortwave infrared measurements: performance comparison of proxy and physics retrieval algorithms, *J. Geophys. Res.*, 117, D10307, 10.1029/2012JD017549, 2012.

Takahashi, T., Sutherland, S. C., Wanninkhof, R., Sweeney, C., Feely, R. A., Chipman, D. W., Hales, B., Friederich, G., Chavez, F., Sabine, C., Watson, A., Bakker, D. C., Schuster, U., Metzl, N., Yoshikawa-Inoue, H., Ishii, M., Midorikawa, T., Nojiri, Y., Körtzinger, A., Steinhoff, T., Hoppema, M., Olafsson, J., Arnarson, T. S., Tilbrook, B., Johannessen, T., Olsen, A., Bellerby, R., Wong, C., Delille, B., Bates, N., and de Baar, H. J.: Climatological mean and decadal change in surface ocean  $p\text{CO}_2$ , and net sea-air  $\{\text{CO}_2\}$  flux over the global oceans, *Deep-Sea Res. Pt. II*, 56, 554–577, 10.1016/j.dsr2.2008.12.009, 2009.

van der Werf, G. R., Randerson, J. T., Giglio, L., Collatz, G. J., Mu, M., Kasibhatla, P. S., Morton, D. C., DeFries, R. S., Jin, Y., and van Leeuwen, T. T.: Global fire emissions and the contribution of deforestation, savanna, forest, agricultural, and peat fires (1997–2009), *Atmos. Chem. Phys.*, 10, 11707–11735, 10.5194/acp-10-11707-2010, 2010.

Wang, J. S., Logan, J. A., McElroy, M. B., Duncan, B. N., Megretskaia, I. A., and Yantosca, R. M.: A 3-D

**Table 1.** A priori sources of carbon dioxide and methane used in the GEOS-Chem model for 2010.

CO <sub>2</sub>	A priori magnitude (Gt year <sup>-1</sup> )	Reference
Fossil fuel	14.8	ODIAC (Oda and Maksyutov, 2011)
Oceans	-5.2	Takahashi et al. (2009)
Biosphere	3.4	CASA (Randerson et al., 1997)
Biomass burning	8.6	GFEDv3 (van der Werf et al., 2010)
CH <sub>4</sub>	A priori magnitude (Tg year <sup>-1</sup> )	Reference
Ruminant animals	92.8	EDGAR 3.2 FT (Olivier et al., 2005)
Coal mining	47.1	EDGAR 3.2 FT (Olivier et al., 2005)
Oil and natural gas production	42.8	EDGAR 3.2 FT (Olivier et al., 2005)
Landfills	44.7	EDGAR 3.2 FT (Olivier et al., 2005)
Rice	68.0	Bloom et al. (2012)
Wetlands	192.0	Bloom et al. (2012)
Biomass burning	19.4	GFEDv3 (van der Werf et al., 2010)
Oceans	15.1	Houweling et al. (1999)
Termites	20.1	Fung et al. (1991)
Hydrates	5.0	Fung et al. (1991)
Soil Sink	-25.2	Fung et al. (1991)

**Table 2.** A priori and a posteriori CH<sub>4</sub> and CO<sub>2</sub> regional land fluxes (natural+anthropogenic) and 1- $\sigma$  uncertainties inferred from GOSAT XCH<sub>4</sub> : XCO<sub>2</sub> and in situ mole fraction measurements. Fluxes inferred from previous work (Fraser et al., 2013; Feng et al., 2011) using an ensemble Kalman Filter are denoted EnKF. CH<sub>4</sub> and CO<sub>2</sub> fluxes are reported as TgCH<sub>4</sub> year<sup>-1</sup> and GtC year<sup>-1</sup>, respectively.

Region	CH <sub>4</sub> Prior		CH <sub>4</sub> Posterior (this work)		CH <sub>4</sub> Posterior (EnKF)		CO <sub>2</sub> Prior		CO <sub>2</sub> Posterior (this work)		CO <sub>2</sub> Posterior (EnKF)	
	Flux	1- $\sigma$	Flux	1- $\sigma$	Flux	1- $\sigma$	Flux	1- $\sigma$	Flux	1- $\sigma$	Flux	1- $\sigma$
Boreal North America	4.1	1.0	4.0	0.9	4.8	0.9	-0.4	0.5	-0.7	0.3	0.1	0.1
Europe	44.5	3.6	31.3	2.4	39.8	2.3	0.5	0.8	0.6	0.4	0.6	0.2
Boreal Eurasia	15.2	2.5	19.3	1.9	15.0	2.5	-0.7	1.0	-1.5	0.9	-0.4	0.2
Temperate North America	58.5	4.1	62.5	3.6	64.9	3.1	0.9	0.8	1.2	0.5	1.4	0.2
Northern Africa	49.6	4.3	65.6	3.5	46.8	4.2	0.3	0.6	0.4	0.5	0.2	0.2
Temperate Eurasia	127.9	11.8	140.2	4.4	124.0	6.5	2.7	0.7	3.4	0.4	3.4	0.2
Tropical South America	45.1	5.6	59.0	3.1	51.1	4.1	-0.2	0.5	0.3	0.3	-0.3	0.3
Tropical Asia	34.6	4.5	40.6	3.2	42.9	3.1	0.7	0.2	0.9	0.2	1.5	0.2
Temperate South America	60.5	5.8	50.9	3.3	55.8	5.6	-0.4	0.6	-0.6	0.4	-0.5	0.3
Southern Africa	46.0	5.1	43.6	3.6	41.4	3.1	-1.4	0.8	-1.9	0.6	0.1	0.2
Australasia	16.7	1.4	17.9	1.3	17.8	1.3	-0.1	0.2	-0.4	0.2	0.7	0.2

model analysis of the slowdown and interannual variability in the methane growth rate from 1988 to 1997, Global Biogeochem. Cy., 18, GB3011, 10.1029/2003GB002180, 2004.

- 420 Worthy, D. E., Platt, J. A., Kessler, R., Ernst, M., and Racki, S.: The Greenhouse Gases Measurement Program, measurement procedures and data quality, in: Canadian Baseline Program; Summary of Progress to 2002, Meteorological Service of Canada, Quebec, 97-120, 2003.

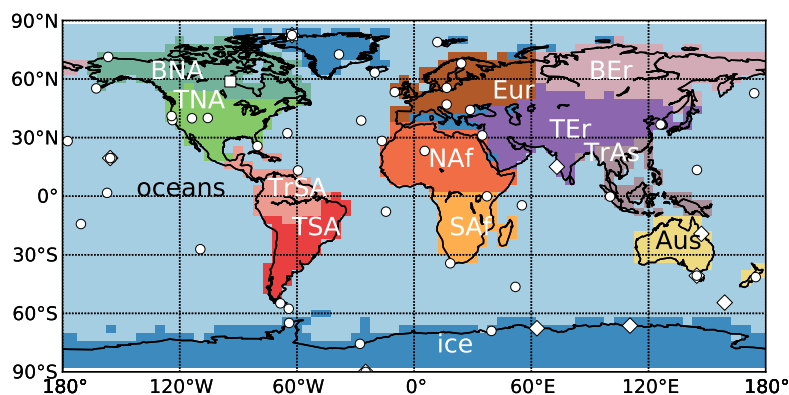


**Fig. 1.** Distribution of the 13 geographical regions for which we estimate  $\text{CO}_2$  and  $\text{CH}_4$  fluxes, and the location of 57 co-operative flask sampling sites with data covering the study period, January–December 2010. The land regions, informed by previous work (Gurney et al., 2002) include: Boreal North America (BNA), Temperate North America (TNA), Tropical South America (TrSA), Temperate South America (TSA), Northern Africa (NAf), Southern Africa (SAf), Boreal Eurasia (BEr), Temperate Eurasia (TEr), Tropical Asia (TrAs), Australasia (Aus), and Europe (Eur). The ground-based measurement sites run by NOAA ESRL, CSIRO GASLAB, and EC are denoted by white circles, white diamonds, and white squares, respectively.

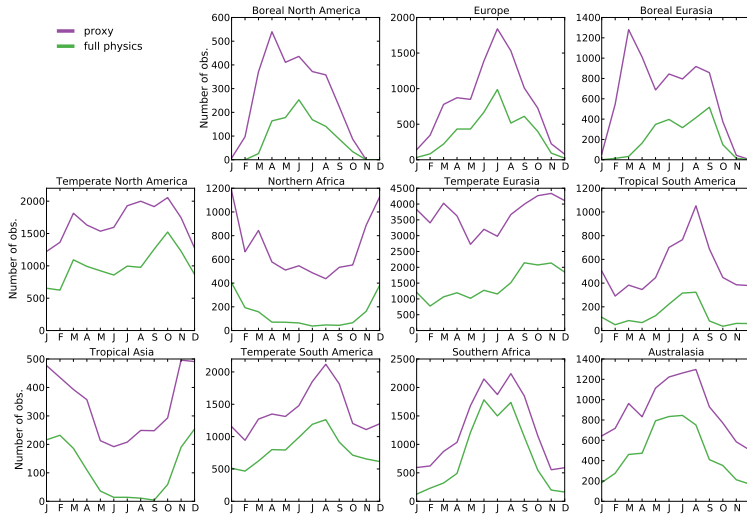


**Fig. 2.** The number of GOSAT observations available per month during 2010 over specific geographical regions (Fig. 1) from the full-physics XCO<sub>2</sub> and proxy XCH<sub>4</sub> retrieval algorithms.

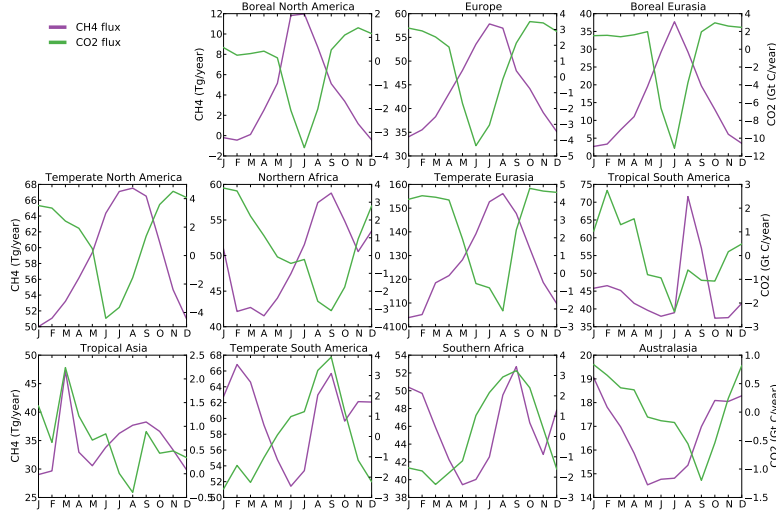


**Fig. 3.** Monthly a priori emissions for CH<sub>4</sub> (TgCH<sub>4</sub>year<sup>-1</sup>) and CO<sub>2</sub> (GtCyear<sup>-1</sup>) for the land regions shown in Fig. 1. Note the different *y*-scales.



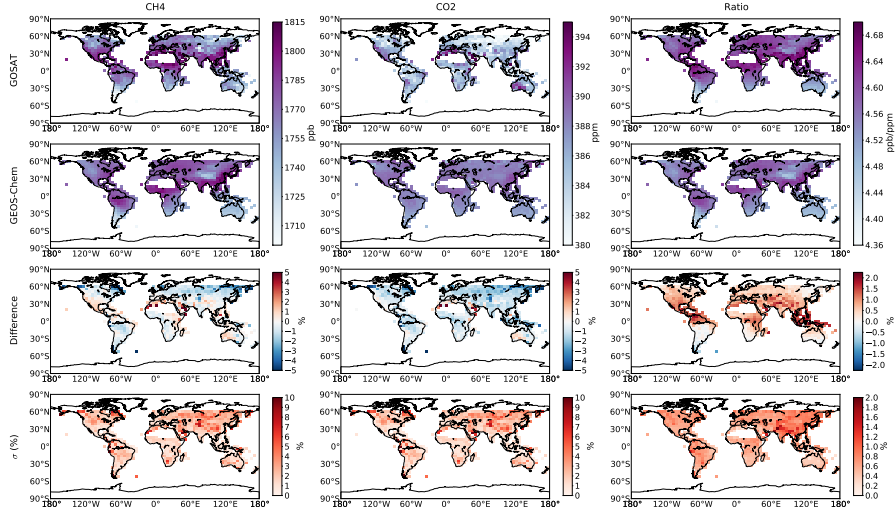


**Fig. 4.** Annual mean GOSAT (top row) and GEOS-Chem model (second row)  $XCH_4$ ,  $XCO_2$ , and  $XCH_4 : XCO_2$  ratio measurements from GOSAT during 2010 averaged on the model  $4^\circ \times 5^\circ$  grid. The third row shows the percentage difference between them (GOSAT minus GEOS-Chem). For  $XCH_4$  and  $XCO_2$ , we truncate at the mean  $\pm 2\sigma$ . The bottom row shows the  $1\text{-}\sigma$  value in the difference as a percentage about the annual mean GOSAT  $XCH_4$ ,  $XCO_2$ , and  $XCH_4 : XCO_2$  data. The model has been sampled at the time and location of the GOSAT observations, and convolved with scene-dependent averaging kernels.

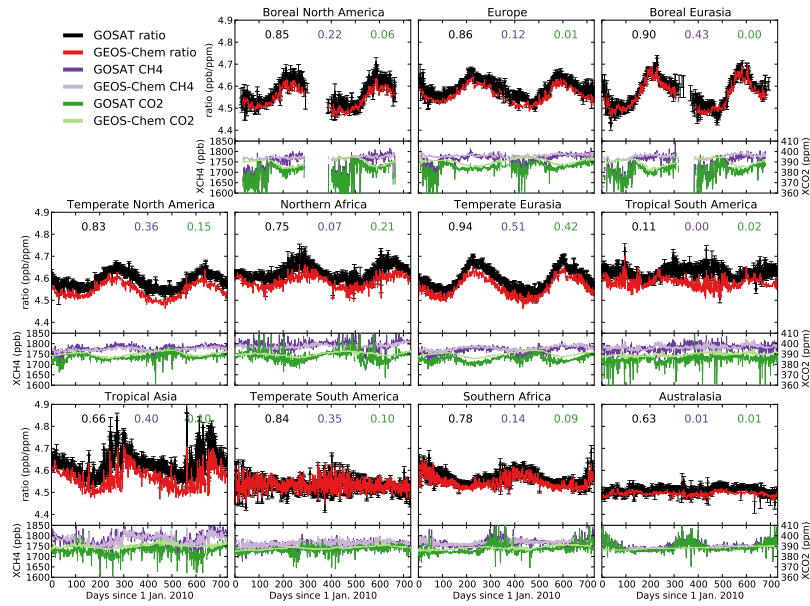


**Fig. 5.** GOSAT and GEOS-Chem daily mean  $XCH_4 : XCO_2$  ratios (top panels) for 2010–2011, averaged over each land region shown in Fig. 1. Squared Pearson correlation coefficients between GOSAT and GEOS-Chem are shown inset for the ratio (black),  $XCH_4$  (purple), and  $XCO_2$  (green). Bottom panels show the corresponding GOSAT and GEOS-Chem daily mean  $XCH_4$  and  $XCO_2$ . The model has been sampled at the time and location of the GOSAT observations, and convolved with scene-dependent averaging kernels.

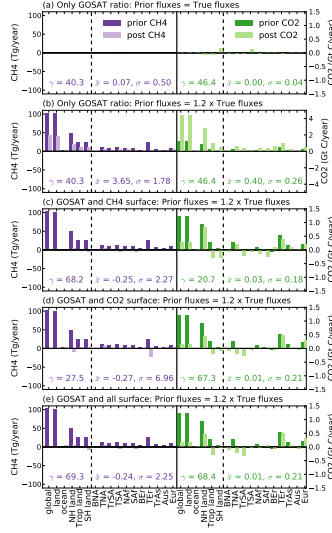


**Fig. 6.** Annual regional flux estimates of CH<sub>4</sub> (left) and CO<sub>2</sub> (right) inferred from various observing system simulation experiments, where values are described as the departure from the corresponding true flux. The first six regions are aggregates: global represents all regional fluxes; land omits the oceans and vice versa; NH land sums fluxes from Boreal and Temperate North America, Europe, and Boreal and Temperate Eurasia; Trop land sums fluxes from Tropical South America, Northern Africa, and Tropical Asia; and SH land sums fluxes from Temperate South America, Southern Africa, and Australasia. The remaining regions are defined in Fig. 1. Experiment (a) for which the a priori and the truth are the same and only GOSAT data are used; experiment (b) is as (a) but the a priori fluxes are 20 % higher than the truth; experiment (c) is as (b) but CH<sub>4</sub> surface flask data are also used; experiment (d) is as (b) but CO<sub>2</sub> surface flask data are also used; experiment (e) is as (b) but CH<sub>4</sub> and CO<sub>2</sub> surface flask data are also used. Note the different y-scale for CO<sub>2</sub> in (b). The error reduction in the global fluxes ( $\gamma$ ), the mean ( $\bar{x}$ ) and standard deviation ( $\sigma$ ) of the difference in the individual regions are shown inset of each panel.

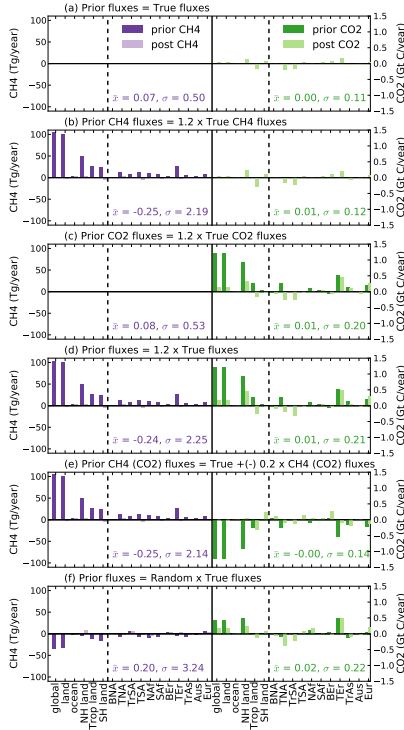


**Fig. 7.** As Fig. 6 but all experiments use CH<sub>4</sub> and CO<sub>2</sub> surface flask data and GOSAT data. Experiment (a) for which a priori fluxes are equal to the true fluxes; experiment (b) for which CH<sub>4</sub> a priori fluxes are 20 % larger than the true fluxes; experiment (c) for which CO<sub>2</sub> a priori fluxes are 20 % larger than the true fluxes; experiment (d) for which CH<sub>4</sub> and CO<sub>2</sub> a priori fluxes are 20 % larger than their true fluxes; experiment (e) for which CH<sub>4</sub> a priori fluxes are 20 % larger and CO<sub>2</sub> a priori fluxes are 20 % smaller than their true fluxes; and experiment (f) for which all a priori fluxes are perturbed stochastically, ranging from -20 % to 20 %, from the true fluxes.

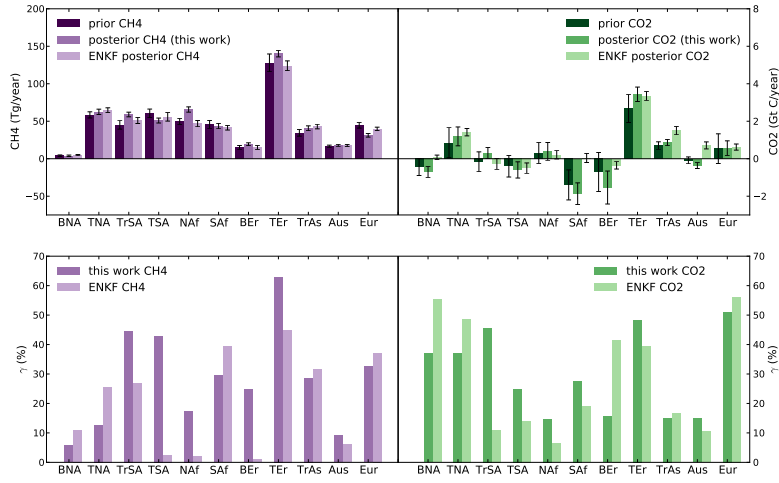


**Fig. 8.** A priori and a posteriori CO<sub>2</sub> and CH<sub>4</sub> regional land fluxes (natural+anthropogenic) inferred from GOSAT XCH<sub>4</sub> : XCO<sub>2</sub> and surface measurements of CO<sub>2</sub> and CH<sub>4</sub> and from XCO<sub>2</sub> or XCH<sub>4</sub> using an ensemble Kalman filter (top) (Feng et al., 2011; Fraser et al., 2013), and the corresponding reduction in uncertainty (bottom), during 2010. Error bars atop of emission estimates represents the 1-σ uncertainty.